# Field-Driven Dynamics of Magnetic Hopfions

David Raftrey and Peter Fischer*
*Materials Sciences Division, Lawrence Berkeley National Laboratory, Berkeley, California 94720, USA*
*and Physics Department, UC Santa Cruz, Santa Cruz, California 95064, USA*

(Received 26 April 2021; revised 27 July 2021; accepted 18 November 2021; published 17 December 2021)

We present micromagnetic simulations on resonant spin wave modes of magnetic Hopfions up to 15 GHz driven by external magnetic fields. A sharp transition is found around 66 mT coinciding with a transition from Hopfions to magnetic torons. The modes exhibit characteristic amplitudes in frequency space accompanied by unique localization patterns in real space and are found to be robust to damping around topological features, particularly vortex lines in Hopfions and Bloch points in torons. The marked differences in spin wave spectra between Hopfions, torons, and target skyrmions can serve as fingerprints in future experimental validation studies of these novel 3D topological spin textures.

DOI: 10.1103/PhysRevLett.127.257201

*Introduction.*—Topological solitons, originally proposed to explain quantized particles in continuous fields [1–3], have recently seen significant attention in condensed matter research, where they appear as stable configurations of the magnetization field in ferromagnetic materials [4,5]. Magnetic skyrmions are prominent examples [6], which exist in two-dimensional chiral magnets resulting from a competition between symmetric exchange (Heisenberg) interactions with antisymmetric exchange, i.e., Dzyaloshinski-Moriya interaction (DMI) [7,8]. Their topological protection makes them attractive candidates for future high-density and low-power spintronic devices [9], but their dynamical behavior is often impaired by topological Hall effects that can be attributed to a gyrovector [10,11]. Recently, the generalization of magnetic skyrmions into the third dimension has opened a path towards more complex and diverse topological solitons, including rings, knots, and links. Recently, several new topological spin structures have been observed including target skyrmions [12,13], skyrmion tubes [14], chiral bobbers [15], vortex rings [16], and Hopfions [17]. Whereas the topological charge that characterizes magnetic skyrmions in two dimensions is the winding number $N_{sk} = \iint d^2 r m \cdot [(\partial m/\partial x) \times (\partial m/\partial y)]$ with $m$ being the magnetization, the corresponding three-dimensional topological solutions can be classified by an additional topological invariant, the Hopf number ($Q_H$). In real space this can be expressed as $Q_H = -\int B \cdot A d^3 r$ with $B$ being the emergent magnetic field from the spin texture and $A$ is the magnetic vector potential [18].

The topological protection in three dimensions is analogous to the process that stabilizes skyrmions in two dimensions. Skyrmions cannot be smoothly unwound into a uniformly magnetized state without passing through a divergent singularity, so they are stable even when they are not in the lowest energy state. Magnetic Hopfions take the form of toroidal knots where each isosurface, the area of a single direction of magnetization, is a loop. The Hopfion's topological invariant is its Hopf number $Q_H$, which is the number of times these isosurfaces are linked [see Fig. 1(c)]. A Hopfion can therefore be considered as a twisted, closed loop of skyrmion string, where the Hopf number is the number of twists [19]. With the application of a static magnetic field along the $z$ axis, the Hopfion constricts in diameter, until at a certain field value, it transforms to the unlinked toron state. The toron is equivalent to a skyrmion tube closed with two opposite Bloch points at the top and bottom [Fig. 1(h)].

Hopfions are predicted to have complex dynamics relevant for spintronic applications [20,21]. Previous computational studies have investigated the dynamics of Hopfions under spin transfer torque [22,23]. Because of their vanishing gyrovector, and therefore vanishing skyrmion Hall effect, under the rigid-body approximation Hopfions can move in a racetrack geometry without deflection, however, they still exhibit complex tumbling and breathing dynamics in three dimensions [23].

In addition to current-induced transport dynamics, spin textures can also be excited by external oscillating fields. The three-dimensional resonances of target skyrmions have been precisely simulated [12], recent studies on skyrmion tubes [24] showed mode-dependent spin wave propagation, and three-dimensional resonance experiments with magnetic field microscopy revealed a complex spin wave spectrum of magnetic "nanovolcanos" [25].

Here we present micromagnetic simulations of the resonant dynamics of magnetic Hopfions confined in chiral magnetic nanopillars up to 15 GHz as a function of external magnetic fields and as a function of damping parameter. We find that Hopfions have unique field-excited dynamics distinct from target skyrmions and torons, which opens a

 

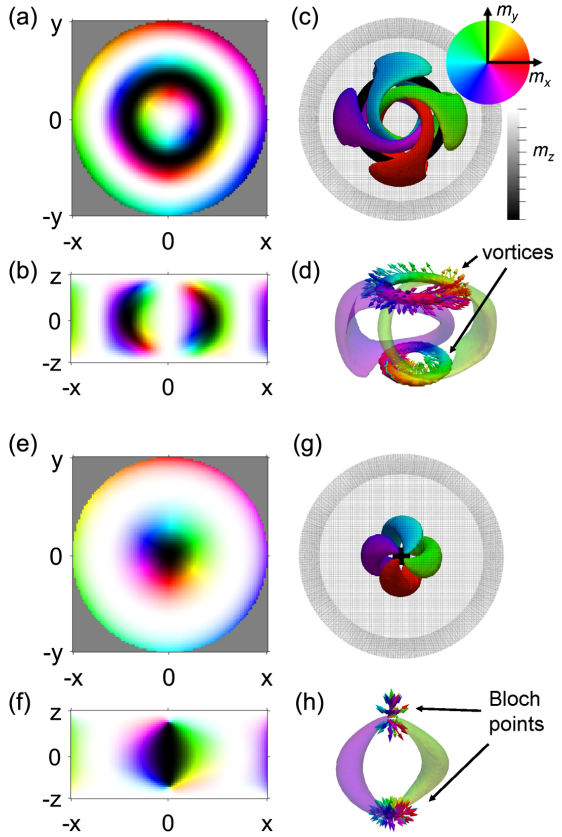


FIG. 1. (a) Magnetization color map of a Hopfion at the $z = 0$ plane. (b) Magnetization color map of Hopfion at the $y = 0$ plane. (c) Hopfion spin textures with linked magnetization isosurfaces. The Hopf invariant or linking number, $Q$, is the number of times the isosurfaces are linked. (d) Detail of Hopfion vortex rings. The vortex rings are a consequence of the Hopf link and do not provide topological protection on their own. The vortex rings are identified by areas with a large $\mathrm{m} \cdot \nabla \times \mathrm{m}$. (e) Magnetization color map of a toron at the $z = 0$ plane. (f) Magnetization color map of toron at the $y = 0$ plane. (g) Toron spin textures with unlinked isosurfaces. A toron has $Q = 0$. (h) Detail of toron Blch points (monopole antimonopole pair). The Bloch points are energetically unfavorable singularities in the divergence $\nabla \cdot \mathrm{m}$ created when the Hopf link is broken. Without the uniform, fixed boundary condition, the Bloch points are destroyed at the upper and lower boundaries of the disk, and the toron becomes a skyrmion tube.

path to discriminating between Hopfions and target skyrmions based on their breathing mode dynamics.

*Simulation details.*—To mimic an experimental scenario [17] a stable Hopfion state was simulated in a disk of chiral ferromagnetic material which is sandwiched between two layers of material with high perpendicular magnetic anisotropy (PMA) (see Fig. 1). The high PMA layers enforce a uniform $m = (0, 0, 1)$ boundary condition on the top and bottom of the disk. Without the uniform boundary condition, the Hopfion expands until it hits the surface and breaks its linked isosurfaces, transforming into the related target skyrmion state [5]. It has been shown that a range of anisotropies can stabilize a bound Hopfion. For simplicity, the simulations shown here employ a fixed spin approximation of the high PMA layer on the top and bottom of the chiral disk. The geometry and material parameters are based on previous theoretical investigations of Hopfions confined in magnetic heterostructures [19,26].

The system was simulated using the MuMax3 GPU accelerated micromagnetic simulator package [27]. Simulations were run in parallel on the Lawrencium supercluster at Lawrence Berkeley National Laboratory in Berkeley, CA.

The local energy density of the chiral disk is given by

$$E = A(\nabla \cdot m)^2 + Dm \cdot (\nabla \times m) - \mu m_s H \cdot m - \frac{1}{2} m_s B_{\mathrm{demag}} \cdot m,$$

where the exchange constant was chosen as $A = 2.19\ \mathrm{pJ/m}$, the DMI constant $D = 0.395\ \mathrm{mJ/m^2}$, and the saturation magnetization $m_s = 384\ \mathrm{kA/m}$. The geometrical dimensions of the chiral disk were height $h = 90$ nm and diameter $d = 200$ nm. The spins in the top and bottom 2 nm layers are fixed in the (0, 0, 1) direction. This specific geometry based on material parameters is needed to stabilize a Hopfion. The dimensions of the disk are set by the chiral period of the material parameters $L = 4\pi A/D = 70$ nm, which rescales the disk geometry in units of L to $h = 1.28$ L and $d = 2.86$ L. These dimensions allow the magnetization to rotate by $2\pi$ from top to bottom of the Hopfion and by $4\pi$ across the diameter of the Hopfion. The cell size was chosen to be 2 nm × 2 nm × 2 nm for a total 450 000 cells per simulation. The demagnetization energy, which helps to stabilize the Hopfion, is included.

To simulate magnetization dynamics, MuMax3 numerically integrates the Landau-Lifshitz-Gilbert equation

$$\dot{m} = -\gamma m \times H + \alpha m \times \dot{m}.$$

A range of damping parameters $\alpha = \{0.001, 0.1\}$ was used to explore the GHz spin wave spectrum of the system and to determine where distinct spin resonances are replaced at high damping by large displacement breathing modes. This range of damping parameters explores the robustness of the modes.

To excite spin wave resonances a pulsed magnetic field was applied. The sinc function, $H(t) = H_{\mathrm{max}}[\sin(2\pi\omega_{\mathrm{max}}t)/2\pi\omega_{\mathrm{max}}t]$, was used as the pulse because its Fourier transform is a step function up to a maximum frequency $\omega_{\mathrm{max}}$, so it excites an unbiased spin wave response from the Hopfion for frequencies up to $\omega_{\mathrm{max}}$ [see Figs. 2(b) and 2(c)] The sinc pulse $\omega_{\mathrm{max}}$ frequency was 15 GHz with an amplitude of 5 mT. The pulse is arbitrarily offset in time to peak at 0.67 ns. Low damping ($\alpha = 0.001$) spin resonance simulations were run for 20 ns with data taken every 17 ps to ensure a resolution below the Nyquist frequency $1/2f$.

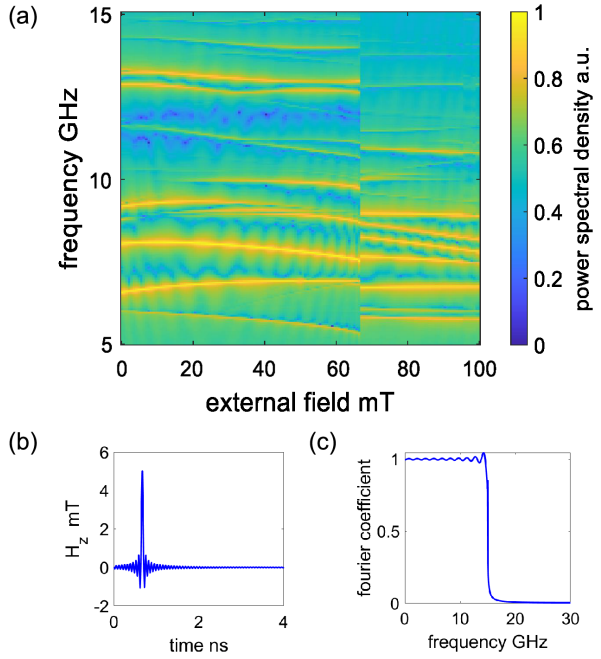


FIG. 2. (a) PSD response of a Hopfion to a sinc pulse under static applied external field (damping parameter $\propto = 0.001$). (b) Magnetic excitation pulse applied in the $x$ direction in the time domain. Pulsed field is the cardinal sign or sinc function. (c) Fourier transform of the excitation pulse in the frequency domain. The sinc function creates a square wave with equal sampling frequency up to a maximum frequency of 15 GHz.

In the high damping $\alpha = 0.1$ simulations a sinusoid, $H(t) = H_{\max} \sin(2\pi\omega_{\max} t)$ with $\omega = 1$ GHz and amplitude of $H_{\max} = 12$ mT was used to excite large amplitude breathing modes. The sinusoid was chosen here instead of the pulse because the pulsed excitation quickly decays under large damping. These high damping simulations were run for 10 ns simulation time with data recorded at increments of 0.1 ns.

*Spin wave breathing mode spectrum under pulsed magnetic field.*—The spin wave resonances were excited by a sinc pulse magnetic field in the $+z$ direction. The resonances are calculated by taking the spatially average fluctuation in $z$ magnetization $\langle \delta m_z(t) \rangle = \langle m_z(t) - m_z(0) \rangle$. The $\langle \delta m_z(t) \rangle$ signal is the Fourier transformed signal to compute the frequency of the resonances.

To examine how a static magnetic field affects the spin wave spectrum, a set of simulation was performed with an additional static magnetic field in $+z$ in addition to a pulse excitation.

Figure 2(a) shows the obtained power spectral density (PSD) response of a Hopfion to the sinc pulse [see Fig. 2(b)] under static applied field where the simulations were performed in steps of 1 mT from 0 to 100 mT. Whereas the Hopfion is stable at zero applied field, some modes frequencies increase while others decrease as the Hopfion constricts under increasing applied field. At a critical field of 66 mT the Hopfion transforms into an unlinked toron state, and this topological transition is accompanied by a discontinuity in the spin wave spectrum. Although a similar number of resonances are present for the Hopfion and toron, which are labeled in Figs. 3(b) and 3(d) with h.1–h.8 for the Hopfion and t.1–t.7 for the toron, the spin wave spectrum is discontinuous across the transition, only mode h.4(t.5) is continuous across the transition.

The width of the resonances modulates under the changing of applied fields, which intensifies when approaching the critical field, implying that Hopfions have a field dependent quality factor to their resonances.

Figures 3(a) and 3(c) show the location in frequency space of the five Hopfion and toron resonances at 50 and 80 mT, respectively. To illustrate each resonance spatially, the amplitude of each spin wave resonance is indicated with isosurfaces in real space, Figs. 3(a) and 3(c).

For the Hopfion, the lowest frequency mode, h.1, has four localized maxima in vertically stacked rings Fig. 3(a). This mode is a breathing resonance as the hopfion expands and contracts. The lowest frequency mode of the toron is also localized in stacked rings, but in the case of the toron only two rings, one at the top and another at the bottom on the disk occur Fig. 3(c). At the Hopfion to toron transition, this mode is discontinuous in both real space, with the transition from four rings to two rings, and in frequency space. The discontinuity of the mode is a consequence of the topological transition from Hopfion to toron. For the Hopfion the mode is localized around the vortex rings, in the case of the toron the mode is located near the Bloch points. At 66 mT when the vortex rings collapse into Bloch points the discontinuous transition of the spin texture causes a discontinuity in the lowest frequency mode.

The next lowest frequency modes, h.2 and t.2, have the largest amplitude at the edge of the disk. This edge mode is a feature of the geometry and would occur even in the case of a uniformly magnetized disk. In the toron state, this mode also excites the spin texture, suggesting that the toron, with its nonzero divergence, is more strongly coupled to the geometry of the system than the smooth and localized Hopfion.

Other modes have complicated distributions across the disk. For all modes the disk edge, Hopfion vortex rings, and toron Bloch points host the highest amplitude spin waves and are surrounded by concentric rings of low-amplitude spin waves. Mode h.4 (t.5) alone is continuous across the Hopfion to toron transition. It is worth noting, that the defects, i.e., the Bloch points or vortex lines, play an important role, as they exhibit a more complicated microstructure than the surrounding bulk, allowing for a wider range of frequencies to exist. This effect is analogous to spin wave channeling by domain walls in two-dimensional systems [28].

*Impact of damping.*—Further insight into the field-driven dynamics of Hopfions and torons is obtained by considering the impact of damping (Fig. 4). The complex spin wave resonances spectrum is only present for a low damping parameter. For a value of $\alpha = 0.001$ there are eight major peaks of varying intensity in the resonance

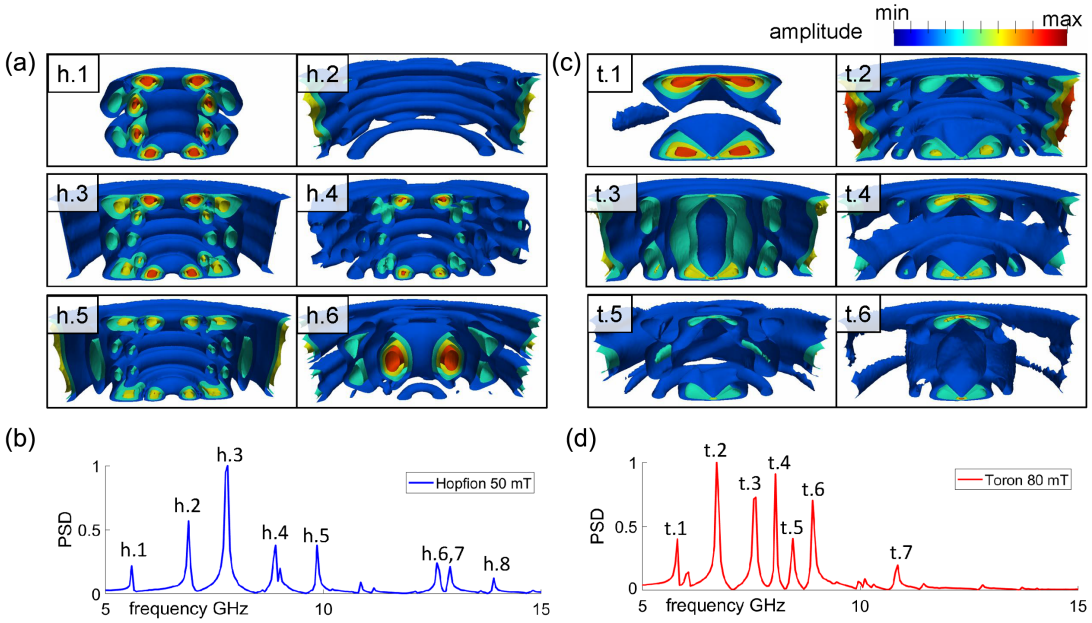


FIG. 3. (a) Localization of the resonant spin-wave modes of a magnetic Hopfion under a 50 mT applied field. Renderings are a half-disk cross section cut through the $x = 0$ plane. Brighter colors indicate increasing spin wave amplitude. Each figure is normalized to have the same highest amplitude (damping parameter $\propto = 0.001$). (b) PSD plot indicating the frequency, and relative amplitude of the Hopfion modes. (c) Localization of the resonant spin wave modes of a magnetic toron under an 80 mT applied field (damping parameter $\propto = 0.001$). (d) PSD plot indicating the frequency of the toron modes.

spectrum (Fig. 4). In contrast, with a large damping parameter $\alpha = 0.1$, the resonant peaks broaden and merge into two or three low frequency modes with broad peaks and reduced amplitude. a single wide band around 4 GHz with reduced amplitude.

In the low damping regime the highest amplitude Hopfion modes are h.2 and h.3. Mode h.3 is localized near the Hopfion vortex rings, and mode h.2 is the edge mode. Under higher damping, the edge mode h.2 merges with the vortex mode and shifts to a lower frequency. This combined edge and vortex mode is the largest mode in the $\alpha = 0.1$ regime.

In the case of the toron, mode t.1 has highest amplitude at $\alpha = 0.001$. Mode t.1 is localized around the Bloch points. The mode with the second highest amplitude, t.2 is localized around the edge of the disk at $\alpha = 0.001$. Under higher damping, $\alpha = 0.01$ t.1 and t.2 have equal amplitude. At an extreme value of damping $\alpha = 0.1$ the dynamics enter a new regime and distinct modes merge into broad, low amplitude resonances. For the toron in the $\alpha = 0.1$ regime, the highest amplitude excitation is localized on the edges of the disk.The Hopfion mode h.2, which has the largest amplitude in the power spectral density is also most robust to damping. It is localized around the vortex lines at

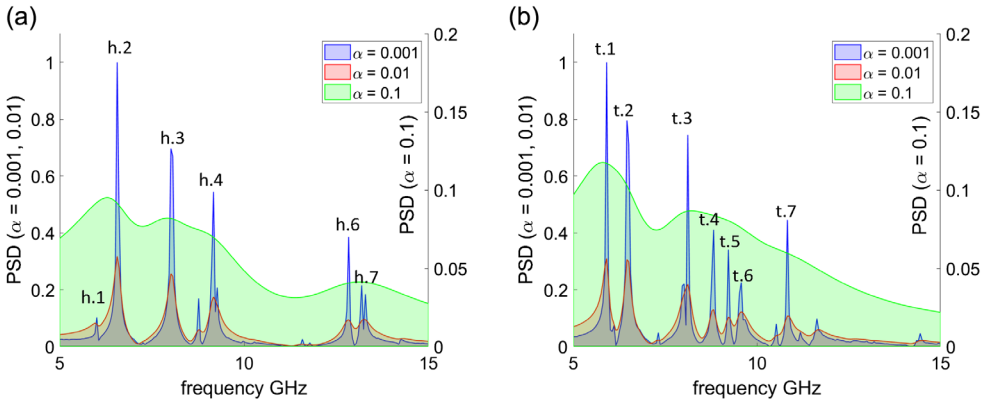


FIG. 4. (a) Hopfion PSD at 0 mT applied field under varying damping parameters. Power spectra lines are normalized to have equal area. PSD with damping parameter $\propto = 0.001$ and 0.01 are on the left axis, PSD with $\propto = 0.1$ is on the right axis. (b) Toron power spectral density at 0 mT applied field (system initialized in toron state, no field switching) under varying damping parameters. PSD with damping parameter $\propto = 0.001$ and 0.01 are on the left axis, PSD with $\propto = 0.1$ is on the right axis.

the top and bottom of the Hopfion, with an additional component in a ring in the center of the Hopfion. The second most robust mode with regard to damping, h.3. is also localized at the vortex line. This topological vortex line not only concentrates the dynamics of the Hopfions, it also increases their robustness under damping.

In the case of the toron the most robust mode, t.2., is localized not only around the Bloch points at the top and the bottom, but also couples to the edge of the disk. The toron's Bloch points are less excitable by an out of plane field than the Hopfion's vortex lines. The modes that are localized only around the Bloch points quickly disappear under damping, while the mode t.2., which is coupled to the edge of the disk, persists.

*Spin wave mode excitations under sinusoidal magnetic field.*—The regime of highly damped oscillations from an off-frequency excitation are of phenomenological interest. Experimental studies are unlikely to have full knowledge of the material parameters necessary to make precise predictions of resonant frequencies. Also, $\alpha$ is strongly dependent on the quality of sample fabrication. The state-of-the-art methods for time-resolved x-ray microscopy in three dimensions do not yet have the resolution in time or space to observe the three-dimensional gigahertz mode reported in Fig. 3. For these reasons, we include this section with findings on field driven response of a Hopfion under experimentally realistic conditions and demonstrate that even under these conditions the response of the Hopfion to an applied sinusoidal field is distinct enough to distinguish it from the related target skyrmion state.

In the highly damped regime ($\alpha = 0.1$) coherent dynamics can still be excited with sinusoidal applied fields, which produces a breathing response to an out of plane field. These responses follow the driving force after a period of transience and die out quickly after the sinusoidal field is removed.

To gain insight into the high damping breathing modes under realistic conditions, we consider the 2D projection of $m_z$ which would be measured in a time-resolved x-ray transmission microscopy type experiment Fig. 5(c).

The radial symmetry of the Hopfion projection allows us to describe $m_z$ with a single vector, $M_z(r)$.

A response vector is computed by taking the change in $M_z$ at each time step,

$$\Delta M_z(r, t_i) = M_z(r, t_i) - M_z(r, t_{i-1}).$$

Taking the outer product of the response vectors and summing over time steps we construct the correlation matrices shown in Figs. 5(a) and 5(b).

$$C_z(r_j, r_k) = \sum_i \Delta M_z(r_j, t_i) \otimes \Delta M_z(r_k, t_i).$$

The bright regions indicate pairs of radii where oscillations are correlated (in phase), the dark regions indicate pairs of radii where the oscillations are anticorrelated (out of phase).

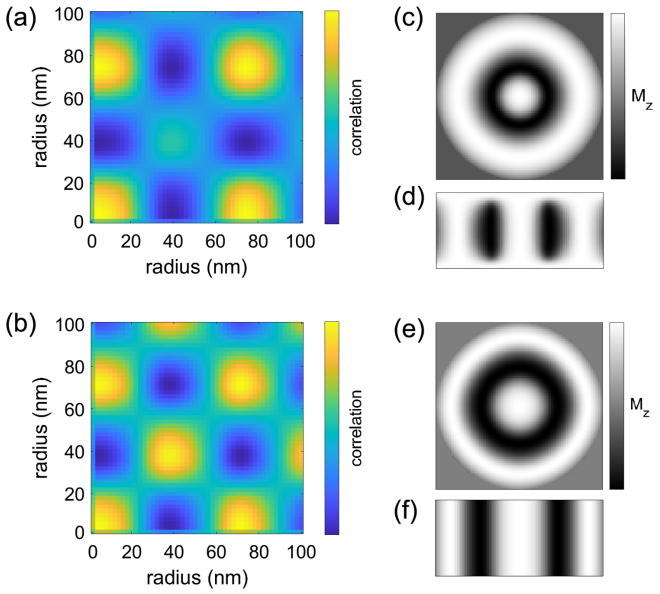


FIG. 5. (a) Hopfion correlation matrix (damping parameter $\propto = 0.1$). (b) Target skyrmion correlation matrix. (c) Hopfion $m_z$ magnetization at the $z = 0$ plane. (d) Hopfion $m_z$ magnetization at the $y = 0$ plane. The Hopfion torus does not reach the top and bottom of the nanopillar. (e) Target skyrmion $m_z$ magnetization at the $z = 0$ plane. In an experimental setting, the Hopfion and target skyrmions are indistinguishable with this static single projection in an XMCD or LTEM type experiment. (f) Target skyrmion $m_z$ magnetization at the $y = 0$ plane. The target skyrmion extends uniformly from the top to the bottom of the nanopillar.

For comparison, this correlation matrix is constructed for the Hopfion as well as the related target skyrmion. The Hopfion response is more localized to the torus, while the target skyrmion correlation is more spread out over the disk, Figs. 5(a) and 5(b). This results from the three-dimensional nature of the Hopfion. The Hopfion is localized to the torus, essentially a one-dimensional closed string. The target skyrmion, on the other hand, is spread out over the entire disk.

The characteristic features in the dynamical behavior shown here could prove useful to differentiate experimentally between a Hopfion and a target skyrmion texture. Figures 5(c) and 5(e) show simulated soft x-ray transmission microscopy data, which are only probing the magnetization projection along the $z$ axis, and cannot distinguish those two spin textures [17], which are different as shown in Figs. 5(d) and 5(f). The distinct correlation matrices of the spin dynamics of these two spin textures would allow the confirmation of three-dimensional character of the spin textures.

*Conclusion.*—We have found strong dependences of the resonant spin wave dynamics in 3D spin textures on their topology. Topological defects such as vortex lines in the case of Hopfions and Bloch points in the case of torons were identified as attractors to localized spin waves in these systems. This extends the idea of domain walls as spin wave channels [28] into three dimensions.

The collapse of vortex lines in Hopfions into Bloch points in torons upon applying external magnetic fields is accompanied by a sharp discontinuity in the spin wave spectrum. Though the modes are discontinuous in frequency space, in real space the spin waves are localized to analogous regions with topological defects (Bloch points and vortex rings) and large Heisenberg energy. These regions serve to focus the spin waves and provide a larger spectrum of excitable frequencies.

The correlated motions of these spin textures are also distinct. The resonances of a Hopfion are more localized at the torus than those of a target skyrmion. The radial breathing modes of the target skyrmion were found to hybridize with modes traveling vertically [12]. Hopfion spin waves are stronger localized but are in general not coupled to the boundary. Therefore, since the Hopfion is shielded by the uniformly magnetized background it is embedded in, the spin wave resonances are more stable against external perturbations, which could open an avenue to harnessing excitations in Hopfion lattices and their breathing mode as information carriers in three-dimensional architectures [29].

The work presented here is limited to findings on the textures' resonant responses to out-of-plane exications. Similar results on the energetics of the Hopfion to toron transition, textures' resonant in respond to in-plane excitations, and Hopfion stability across material parameters are available in the supplemental information [30].

This work was funded by the U.S. Department of Energy, Office of Science, Office of Basic Energy Sciences, Materials Sciences and Engineering Division under Contract No. DE-AC02-05-CH11231 (Non-equilibrium magnetic materials program MSMAG). This research used the Lawrencium computational cluster resource provided by the IT Division at the Lawrence Berkeley National Laboratory, supported by the U.S. Department of Energy, Office of Science, Office of Basic Energy Sciences under Contract No. DE-AC02-05CH11231)

*Corresponding author.
PJFischer@lbl.gov

[1] N. Manton and P. Sutcliffe, *Topological Solitons* (Cambridge University Press, Cambridge, England, 2004).
[2] J.-S. B. Tai, P. J. Ackerman, and I. I. Smalyukh, Proc. Natl. Acad. Sci. U.S.A. **115**, 921 (2018).
[3] R. A. Battye and P. M. Sutcliffe, Phys. Rev. Lett. **81**, 4798 (1998).
[4] P. Sutcliffe, Phys. Rev. Lett. **118**, 247203 (2017).
[5] P. Sutcliffe, J. Phys. A **51**, 375401 (2018).
[6] K. Everschor-Sitte, J. Masell, R. M. Reeve, and M. Kläui, J. Appl. Phys. **124**, 240901 (2018).
[7] I. Dzyaloshinsky, J. Phys. Chem. Solids **4**, 241 (1958).
[8] T. Moriya, Phys. Rev. **120**, 91 (1960).
[9] A. Fert, V. Cros, and J. Sampaio, Nat. Nanotechnol. **8**, 152 (2013).
[10] W. Jiang, X. Zhang, G. Yu, W. Zhang, X. Wang, M. Benjamin Jungfleisch, John E. Pearson, X. Cheng, O. Heinonen, K. L. Wang, Y. Zhou, A. Hoffmann, and Suzanne G. E. te Velthuis, Nat. Phys. **13**, 162 (2017).
[11] K. Litzius, I. Lemesh, B. Krüger, P. Bassirian, L. Caretta, K. Richter, F. Büttner, K. Sato, O. A. Tretiakov, J. Förster, R. M. Reeve, M. Weigand, I. Bykova, H. Stoll, G. Schütz, G. S. D. Beach, and M. Kläui, Nat. Phys. **13**, 170 (2017).
[12] F. Zheng, H. Li, S. Wang, D. Song, C. Jin, W. Wei, A. Kovács, J. Zang, M. Tian, Y. Zhang, H. Du, and R. E. Dunin-Borkowski, Phys. Rev. Lett. **119**, 197205 (2017).
[13] N. Kent, R. Streubel, C.-H. Lambert, A. Ceballos, S.-G. Je, S. Dhuey, M.-Y. Im, F. Büttner, F. Hellman, S. Salahuddin, and P. Fischer, Appl. Phys. Lett. **115**, 112404 (2019).
[14] M. T. Birch *et al.*, Nat. Commun. **11**, 1726 (2020).
[15] F. S. Zheng, F. N. Rybakov, A. B. Borisov, D. S. Song, S. S. Wang, Z. A. Li, H. F. Du, N. S. Kiselev, J. Caron, A. Kovacs, M. L. Tian, Y. H. Zhang, S. Blugel, and R. E. Dunin-Borkowski, Nat. Nanotechnol. **13**, 451 (2018).
[16] C. Donnelly, K. L. Metlov, V. Scagnoli, M. Guizar-Sicairos, M. Holler, N. S. Bingham, J. Raabe, L. J. Heyderman, N. R. Cooper, and S. Gliga, Nat. Phys. **17**, 316 (2021).
[17] N. Kent, N. Reynolds, D. Raftrey, I. T. G. Campbell, S. Virasawmy, S. Dhuey, R. V. Chopdekar, A. Hierro-Rodriguez, A. Sorrentino, E. Pereiro, S. Ferrer, F. Hellman, P. Sutcliffe, and P. Fischer, Nat. Commun. **12**, 1562 (2021).
[18] J. H. C. Whitehead, Proc. Natl. Acad. Sci. U.S.A. **33**, 117 (1947).
[19] Y. Liu, R. K. Lake, and J. Zang, Phys. Rev. B **98**, 174437 (2018).
[20] B. Göbel, C. A. Akosa, G. Tatara, and I. Mertig, Phys. Rev. Research **2**, 013315 (2020).
[21] M. Lonsky and A. Hoffmann, APL Mater. **8**, 100903 (2020).
[22] X. S. Wang, A. Qaiumzadeh, and A. Brataas, Phys. Rev. Lett. **123**, 147203 (2019).
[23] Y. Liu, W. Hou, X. Han, and J. Zang, Phys. Rev. Lett. **124**, 127204 (2020).
[24] S. Seki, M. Garst, J. Waizner, R. Takagi, N. D. Khanh, Y. Okamura, K. Kondou, F. Kagawa, Y. Otani, and Y. Tokura, Nat. Commun. **11**, 256 (2020).
[25] O. V. Dobrovolskiy, N. R. Vovk, A. V. Bondarenko, S. A. Bunyaev, S. Lamb-Camarena, N. Zenbaa, R. Sachser, S. Barth, K. Y. Guslienko, A. V. Chumak, M. Huth, and G. N. Kakazei, Appl. Phys. Lett. **118**, 132405 (2021).
[26] J.-S. B. Tai and I. I. Smalyukh, Phys. Rev. Lett. **121**, 187201 (2018).
[27] A. Vansteenkiste, J. Leliaert, M. Dvornik, M. Helsen, F. Garcia-Sanchez, and B. Van Waeyenberge, AIP Adv. **4**, 107133 (2014).
[28] K. Wagner, A. Kákay, K. Schultheiss, A. Henschke, T. Sebastian, and H. Schultheiss, Nat. Nanotechnol. **11**, 432 (2016).
[29] A. Fernández-Pacheco, R. Streubel, O. Fruchart, R. Hertel, P. Fischer, and R. P. Cowburn, Nat. Commun. **8**, 15756 (2017).
[30] See Supplemental Material at http://link.aps.org/supplemental/10.1103/PhysRevLett.127.257201 for simulations on the energy of the Hopfion and toron states, the response to in-plane excitations, and material parameters.